NANO: Brief Reports and Reviews
Vol. 3, No. 1 (2008) 55–63

World Scientific
www.worldscientific.com

ANALYTICAL AND NUMERICAL MODELING METHODS FOR IMPEDANCE ANALYSIS OF SINGLE CELLS ON-CHIP

TAO SUN*, NICOLAS G. GREEN and HYWEL MORGAN†
Nanoscale Systems Integration Group
School of Electronics and Computer Science
University of Southampton, United Kingdom, SO17, 1BJ
**ts04r@ecs.soton.ac.uk*
†*hm@ecs.soton.ac.uk*

Received 24 April 2007
Revised 12 December 2007

Electrical impedance spectroscopy (EIS) is a noninvasive method for characterizing the dielectric properties of biological particles. The technique can differentiate between cell types and provide information on cell properties through measurement of the permittivity and conductivity of the cell membrane and cytoplasm. In terms of lab-on-a-chip (LOC) technology, cells pass sequentially through the microfluidic channel at high speed and are analyzed individually, rather than as traditionally done on a mixture of particles in suspension. This paper describes the analytical and numerical modeling methods for EIS of single cell analysis in a microfluidic cytometer. The presented modeling methods include Maxwell's mixture theory, equivalent circuit model and finite element method. The difference and advantages of these methods have been discussed. The modeling work has covered the static case — an immobilized cell in suspension and the dynamic case — a moving cell in the channel.

Keywords: Impedance spectroscopy; single cell analysis; microfluidic cytometer.

1. Introduction

With the rapid development of micro-fabrication technology, the lab-on-a-chip (LOC) begins to have a significant impact in the field of biochemistry, biomedical engineering and bioelectronics. Such devices promise portability, convenient operation, low cost and high throughput analysis. For bio-particle analysis, a number of discrete processes are required, such as manipulation, separation, characterization and identification. The electrical techniques used in LOC are either electrophoretic/electroosmotic methods, which require high voltages and operate at DC, or those based on AC electrokinetic method,[1] which include dielectrophoresis (DEP),[2–5] traveling wave dielectrophoresis (TWDEP),[6–8] electrorotation (ROT).[9–12] Apart from these methods, electrical impedance spectroscopy (EIS) is widely used to identify single particles in a microfluidic system at the advantages of high throughput, noninvasive and label-free.[13–19] If the AC excitation voltage is applied across a range of frequencies, the technique allows the measurements on both surface and internal electrical properties of the particles.

Figure 1 shows the schematic of a microfluidic cytometer using EIS technique for single cells analysis. The microchip was fabricated using photolithography and full wafer thermal bonding. 100 nm of Pt

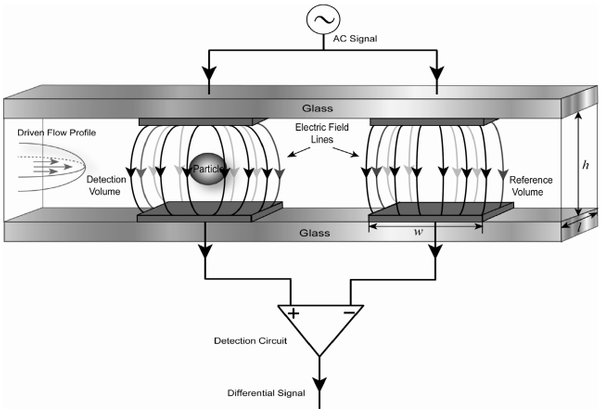

Fig. 1. Schematic of the microfluidic cytometer used for single cell electrical impedance spectroscopy (EIS). As a particle passes through the channel, the measurement is performed using a differential scheme. The two sensing volumes are positioned by the two pairs of parallel facing electrodes. w is the width and l the length of the electrodes. h is the height of the channel.

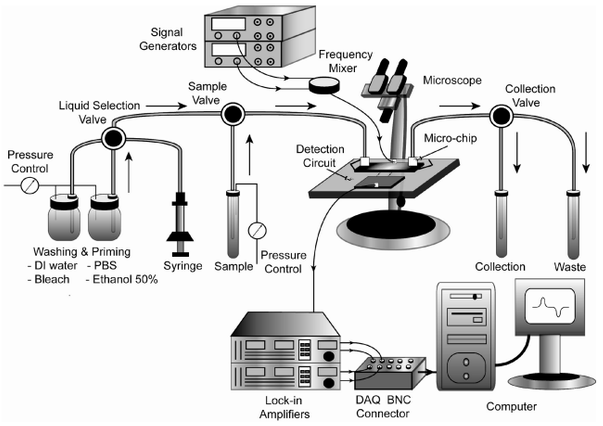

Fig. 2. The measurement setup for impedance analysis of a fluid sample.

was evaporated onto the substrate and patterned the microelectrodes. The parallel facing electrode design was chosen for the experiments because of its improved measurement sensitivity.[20] The microelectrodes were fabricated with sizes similar to the cells (typically 20 μm). Microfluidic channels were made of a thick photosensitive polymide precursor. The width and the height of the microchannel is 20 μm. Individual chips were released from the wafers via dicing with a diamond saw. Inlet and outlet holes were drilled in the individual chips to allow fluidic access. More details of the chip fabrication were reported by Holmes *et al.*[21]

In the experiments, an AC excitation voltage is applied to the two top microelectrodes, generating an electric field within the microfluidic channel. Two pairs of electrodes are used to define two closely positioned detection volumes so that a differential measurement can be made. One pair of electrodes is used to measure the electrical signal induced by the particle and the other is used as a reference. The differential signal is measured using a custom-made detection circuit. Particles flow through the channel under pressure-driven flow at a constant velocity. As they pass through the channel one by one, they modify the current lines through each of the two detection volumes in turn. The signal detected by the electronics depends on the cell properties such as size and the intrinsic dielectric properties of the cell (e.g., membrane capacitance and cytoplasm resistance). The differential measurement scheme shown in Fig. 1 is able to measure cell speed and also reduce measurement noise due to the variations in temperature or composition of the fluid.

Figure 2 shows the instrumentation of the whole impedance measurement system. In this diagram, for the fluidic setup, a rotary valve selects the different washing or priming liquids. Additionally, a motorized syringe pump is used for fast purging of the whole line with high pressure to prevent channel clogging. A sample valve selects the cleaning liquid and sample. Pressure control of the sample tube is provided by a high-precision pressure regulator. The height and level of the liquid in the collection vials is set so as to produce a small back-flow when atmospheric pressure is applied on the sample.

For electrical impedance detection, two AC excitation signals at low and high frequencies are mixed and applied to the cytometer chip. The electrical current from the electrodes is converted into a voltage signal by the detection circuit, composed of a trans-impedance amplifier, followed by a differential amplifier to give the final signal. Two lock-in amplifiers demodulate the in-phase and out-of-phase signals at each frequency, whilst rejecting noise at the other frequencies. Data is sample with a 16-bit data acquisition card. Data analysis is performed using custom software to extract the impedance information, such as the magnitude and phase.

The impedance measurement setup presented above has been experimentally proved to be an efficient and robust system for high speed single cells analysis.[15,16,18,19] In order to have a clear and deep understanding of the measured data and the bio-physics behind the experimental phenomenon,

it is important to develop theoretical models to study the electrical response of the cells in the system. In this paper, we present three analytical or numerical methods for the modeling work on single cell in suspension. The features and the application limitations of each method will be discussed in the following sections.

2. Modeling on Single Cell in Suspension

Colloidal particles and biological cells in suspension are heterogeneous systems. The characterization of the dielectric properties of these heterogeneous systems using dielectric/impedance spectroscopy can be traced back to 1900s.[22–24] The theory linking to this research field is first derived by Maxwell,[25] which is the well-known Maxwell's mixture theory (MMT). In this section, we will start with the introduction of MMT and then we will apply it to derive the impedance of the suspending system containing a single cell in suspension between the two parallel facing electrodes by taking the fringing field effect into account. Then we will analyze the electrical response of the same system in the engineering point of view by using the equivalent circuit model (ECM). Finally, numerical modeling solution using finite element method (FEM) is presented.

2.1. *Maxwell's mixture theory*

MMT gives the equivalent complex permittivity of the heterogeneous system in the complex frequency domain. In terms of a single-shelled spherical cell model (as shown in Fig. 3(a)) in suspension, the equivalent complex permittivity of the mixture is:

$$\tilde{\varepsilon}_{\text{mix}} = \tilde{\varepsilon}_m \frac{1 + 2\varphi \tilde{f}_{\text{CM}}}{1 - \varphi \tilde{f}_{\text{CM}}}, \tag{1}$$

where, $\tilde{\varepsilon}_{\text{mix}}$, $\tilde{\varepsilon}_m$, $\tilde{\varepsilon}_p$ are the complex permittivity for the mixture, suspending medium and the cell, respectively. φ is the volume fraction, which is defined as the volume ratio of the cell to the detection area, and $\tilde{f}_{\text{CM}}$ is the complex Clausius-Mossotti factor:

$$\tilde{f}_{\text{CM}} = \frac{\tilde{\varepsilon}_p - \tilde{\varepsilon}_m}{\tilde{\varepsilon}_p + 2\tilde{\varepsilon}_m}. \tag{2}$$

For a single-shelled spherical cell model, $\tilde{\varepsilon}_p$ is:

$$\tilde{\varepsilon}_p = \tilde{\varepsilon}_{\text{mem}} \frac{\gamma^3 + 2\left(\dfrac{\tilde{\varepsilon}_i - \tilde{\varepsilon}_{\text{mem}}}{\tilde{\varepsilon}_i + 2\tilde{\varepsilon}_{\text{mem}}}\right)}{\gamma^3 - \left(\dfrac{\tilde{\varepsilon}_i - \tilde{\varepsilon}_{\text{mem}}}{\tilde{\varepsilon}_i + 2\tilde{\varepsilon}_{\text{mem}}}\right)} \tag{3}$$

with $\gamma = R/(R-d)$.

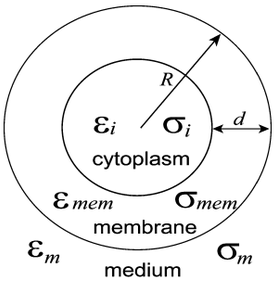

(a)

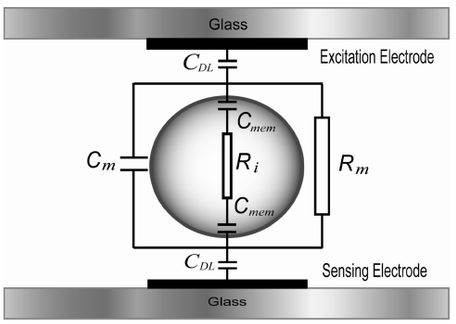

(b)

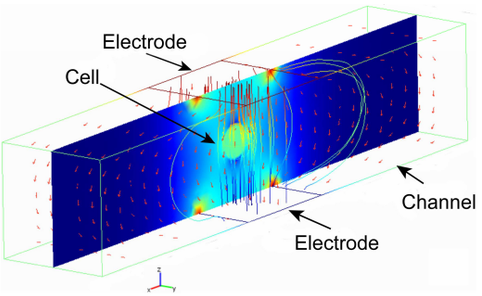

(c)

Fig. 3. (a) Schematic of single-shelled spherical cell in suspension. (b) A diagram showing the equivalent circuit model for a single cell in suspension. R_m and C_m are the equivalent resistance and capacitance of the medium, respectively. C_{mem} is the equivalent capacitance of the cell membrane. R_i is equivalent resistance of the cell cytoplasm. C_{DL} is the electrical double layer capacitance. (c) A diagram showing the numerical simulations of the electric field distribution in the channel, as the cell sits in the central using finite element method (FEM) in Comsol Multiphysics.

Here $\tilde{\varepsilon}_{\text{mem}}$ and $\tilde{\varepsilon}_i$ are the complex permittivity of the cell membrane and cytoplasm, respectively. R is the radius of the cell and d ($d \ll R$) is the thickness of the membrane.

MMT gives an elegant description of the dielectric properties of the mixture in low volume fraction cases ($\varphi < 10\%$). Moreover, the characteristic relaxation time constants in the suspending system

due to the interfacial polarization at the interface between the medium and the cell can be identified through MMT.[26,27] However, the derivation of MMT is based on the assumption that the cell is locating in a homogeneous external electric field. In the cytometer case, the parallel facing electrodes (Fig. 1) generates a nonhomogeneous field distribution within the micro-channel due to the fringing field effect. This makes that the application of MMT for evaluating the impedance of the system is only valid, when the cell sits in the center between the two facing electrodes (as shown in Fig. 1), where the field distribution is quasi-homogeneous.[20]

The complex impedance $\tilde{Z}_{\text{mix}}$ of the suspending system is associated with the equivalent complex permittivity of the mixture by the geometrical parameters of the cytometer:

$$\tilde{Z}_{\text{mix}} = \frac{1}{j\omega\tilde{\varepsilon}_{\text{mix}} l\kappa}\,. \tag{4}$$

In Eq. (4), l is the length of the electrode as shown in Fig. 1. κ is the cell constant of the chip which depends on the ratio of electrode width (w) to the channel height (h). If we ignore the fringing field effect (homogeneous field case), κ simply equals to w/h. In order to consider the fringing field effect, Schwarz–Christoffel mapping method is required to solve the expression of κ[20]:

$$\kappa = \frac{K(k)}{K'(k)}\,, \quad k = \tanh\left(\frac{\pi w}{2h}\right), \tag{5}$$

where $K(k)$ is the complete elliptic integral of the first kind, $K'(k)$ is the complementary integrals and k is the modulus of the elliptic function.

Equation (4) gives the analytical complex impedance expression of the suspending system using MMT. As mentioned before, MMT is only valid in the low volume fraction cases. For high concentration situations, Hanai's equation[28] should be adopted in the analysis.

2.2. *Equivalent circuit model*

From an electrical engineer rather than a physicist's point of view, the study of the electrical response of a cell in a suspension will be much easier to be understood using an equivalent circuit model (ECM) as shown in Fig. 3(b). In this circuit model, the impedance of the medium is represented by a resistor and capacitor in parallel. For a viable cell, the membrane has a very low conductivity and can be modeled as a capacitor. At low frequencies, this prevents current flowing through the cell. The cell cytoplasm is represented by a resistor and the capacitance can be ignored to a first approximation. Additionally, in Fig. 3(b) the electrode–electrolyte interface impedance is modeled as a capacitor, C_{DL}, which is known as the electrical double layer (EDL) effect.[1]

Therefore, the electrical response of the system can be clearly illustrated in different frequency ranges. In the low frequency range ($< 1\,\text{MHz}$), the electrical response of the system is dominated by the EDL capacitance. The sensitivity of impedance detection of a cell is very low in this frequency range, because most of the applied voltage is dropped across the EDL. As the frequency increases, the electrode–electrolyte interface impedance (EDL capacitance) is gradually reduced and the sensitivity of the system improves, and the absolute amplitude of the signal depends on cell size. In the frequency range of 1–100 MHz, the electric field gives rise to a polarization of the interface between the cell and the suspending medium, which is measured as a change in the impedance. As the frequency increases the capacitance of the cell membrane is effectively short-circuited and the electrical response then depends on the internal properties of the cell (i.e., cytoplasm).

The values of the individual electrical components in the circuit model are determined by the cell size, dielectric properties of the medium and the cell, the volume fraction and also the geometrical parameters of the chip[29,30]:

$$R_m = \frac{1}{\sigma_m(1 - 3\varphi/2) l\kappa}\,, \tag{6}$$

$$C_m = \varepsilon_m \frac{2\varepsilon_m + \varepsilon_i - 2\varphi(\varepsilon_m - \varepsilon_i)}{2\varepsilon_m + \varepsilon_i + \varphi(\varepsilon_m - \varepsilon_i)} l\kappa\,, \tag{7}$$

$$C_{\text{mem}} = \frac{9\varphi R C_{\text{mem},0}}{2}\kappa l\,, \tag{8}$$

$$R_i = \frac{4\left(\dfrac{1}{2\sigma_m} + \dfrac{1}{\sigma_i}\right)}{9\varphi\kappa l} \tag{9}$$

with

$$C_{\text{mem},0} = \frac{\varepsilon_{\text{mem}}}{d}\,, \tag{10}$$

where $C_{\text{mem},0}$ is the specific membrane capacitance (capacitance per unit area).

Without considering the EDL capacitance, the complex impedance of the suspending system is

given by:

$$\tilde{Z}_{\text{mix}} = \frac{R_m(1 + j\omega R_i C_{\text{mem}})}{j\omega R_m C_{\text{mem}} + (1 + j\omega R_i C_{\text{mem}})(1 + j\omega R_m C_m)}. \tag{11}$$

The significance of ECM is that the model can be integrated with the schematic of the differential measurement circuit in commercial circuit analysis software, i.e., PSpice (Cadence, Inc., USA) to perform circuit level simulations of the whole measurement system. The comparisons between the circuit simulation results and the experimental data are helpful to find the optimal frequency to achieve the maximum measurement sensitivity and also determine the structure and internal properties of the cells.[30]

2.3. *Finite element method*

Nowadays, numerical simulations using finite element method (FEM) become a widely accepted and easy-used tool in the field of bio-MEMS, due to the well development in commercial FEM softwares, such as: FEMLAB/Comsol Multiphysics, Flexpde, CFD-ACE+. The general steps of using commercial FEM software can be summarized as below:

(i) Define a physical geometry to address the problem.
(ii) Set the boundary conditions in the defined geometry and try to simplify the geometry, utilizing the symmetrical boundary conditions.
(iii) Set the mesh density and expected convergence of the numerical solutions
(iv) Post data/image processing after solving the problem.

It is easy to use commercial FEM softwares to start solving a problem but difficult to get confident and reliable solutions, since the accuracy of numerical solutions strongly depend on the mesh density, the computational capability of the PC and the geometry of specific problems.

In terms of modeling our suspending system (a single-shelled spherical cell between two facing electrodes), the FEM simulations get problematic even in the first step: defining a single-shelled spherical cell. This is because there is a large difference in the geometry ratios, for example a thin cell membrane (5 nm) compared with a cell (5 μm). In order to accurately evaluate the cell with a thin membrane, we derive the equivalent permittivity and conductivity of the cell according to MMT. By separating the real and imaginary parts of Eq. (3), the equivalent permittivity (ε_p) and conductivity (σ_p) for a single-shelled cell are:

$$\varepsilon_p = \frac{\omega(\lambda_2\lambda_4 + \lambda_1\lambda_3\omega^2)\varepsilon_{\text{mem}} + \omega(\lambda_1\lambda_4 - \lambda_2\lambda_3)\sigma_{\text{mem}}}{\omega(\omega^2\lambda_3^2 + \lambda_4^2)}, \tag{12}$$

$$\sigma_p = \frac{-\omega^2(\lambda_1\lambda_4 - \lambda_2\lambda_3)\varepsilon_{\text{mem}} + (\lambda_2\lambda_4 + \lambda_1\lambda_3\omega^2)\sigma_{\text{mem}}}{\omega^2\lambda_3^2 + \lambda_4^2} \tag{13}$$

with coefficients λ_1, λ_2, λ_3 and λ_4:

$$\lambda_1 = \gamma^3(\varepsilon_i + 2\varepsilon_{\text{mem}}) + 2(\varepsilon_i - \varepsilon_{\text{mem}}), \tag{14a}$$

$$\lambda_2 = \gamma^3(\sigma_i + 2\sigma_{\text{mem}}) + 2(\sigma_i - \sigma_{\text{mem}}), \tag{14b}$$

$$\lambda_3 = \gamma^3(\varepsilon_i + 2\varepsilon_{\text{mem}}) - (\varepsilon_i - \varepsilon_{\text{mem}}), \tag{14c}$$

$$\lambda_4 = \gamma^3(\sigma_i + 2\sigma_{\text{mem}}) - (\sigma_i - \sigma_{\text{mem}}). \tag{14d}$$

The cell is modeled as a solid homogeneous sphere with equivalent permittivity and conductivity given by Eqs. (12) and (13). Fixed mesh parameters were set in the sub-domains (cell and suspending medium) and on the boundaries (surface of electrode and the interface between the cell and surrounding medium). The value of the current is determined by integration at the central symmetry plane rather than the surface of the electrode, since the electric fields are extremely high at the electrode edges, producing significant numerical errors. The complex impedance of the cell in suspension is derived by dividing the applied voltage by the value of the complex current. Figure 3(c) shows the FEM modeling of the 3D electric field distribution in the system using Comsol Multiphysics 3.2 (Comsol, Inc.).

Although the FEM requires an expensive computational capability to obtain accurate results, the advantage of FEM is that the analysis can be performed for any arbitrary position of the cell in the channel to obtain the impedance variation as the cell flows through the cytometer.

3. Results and Discussion

In this section, the simulation results for the suspending system containing single-shelled spherical cell from the above three methods are presented and comparisons are performed. The basic simulation

parameters of the channel, medium and the cell are set as: $w = h = l = 20\,\mu$m, $\varepsilon_o = 8.854\times10^{-12}\,\mathrm{Fm}^{-1}$, $d = 5\,$nm, $\varepsilon_m = 80\,\varepsilon_o$, $\varepsilon_{\mathrm{mem}} = 5.647\,\varepsilon_o$, $\varepsilon_i = 60\,\varepsilon_o$, $\sigma_m = 1.6\,\mathrm{Sm}^{-1}$, $\sigma_{\mathrm{mem}} = 10^{-8}\,\mathrm{Sm}^{-1}$, $\sigma_i = 0.6\,\mathrm{Sm}^{-1}$, $R = 3\,\mu$m.

3.1. *Comparisons between MMT and ECM*

The impedance variations due to the changes in the size of the cell have been discussed in Ref. 30 and the simulation results from MMT and ECM show a good agreement in small size cells. Here, the influences on the impedance from the changes in the internal properties (including cell membrane capacitance and cytoplasmic conductivity) of the cell are discussed. This may be more interesting than the pure cell size effect in the single cell analysis, since it allows a comprehensive study on the individual cell behavior from the environmental stimuli. Figures 4(a) and 4(b) show the impedance spectra variations of the suspending system due to the changes in cell specific membrane capacitance and cytoplasmic conductivity, respectively. The calculation results are shown both from MMT (Eq. (4)) by lines and from ECM (Eq. (11)) by dots. Excellent agreements between MMT and ECM can be observed.

Since cell membrane is a poorly conducting thin layer (very low conductivity) and it separates the cell cytoplasm and the suspending medium, in AC electric field, it takes time to charge the cell membrane. The relaxation phenomenon corresponding to this process is termed as the β-relaxation.[31] There are two relaxation frequencies in the frequency domain (or time constants in time domain) for characterizing this relaxation process.[26,27] The lower relaxation frequency (typically between 1–10 MHz) corresponds to the charging process at the interface between the cell membrane and the medium. Therefore, the impedance measurements in this frequency range give the dielectric properties of cell membrane as shown in Fig. 4(a). The higher relaxation frequency (typically above 10 MHz) corresponds to the charging process between the medium and the cell cytoplasm, as the cell membrane is effectively short-circuited. Therefore the impedance measurements above 10 MHz provide the dielectric properties of cell cytoplasm as shown in Fig. 4(b).

The existence of electrical double layer (EDL) over the surface of the electrodes gives a strong impact on the impedance measurements in the

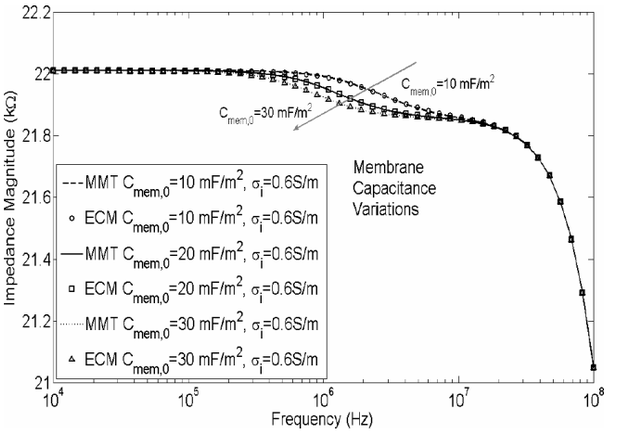

(a)

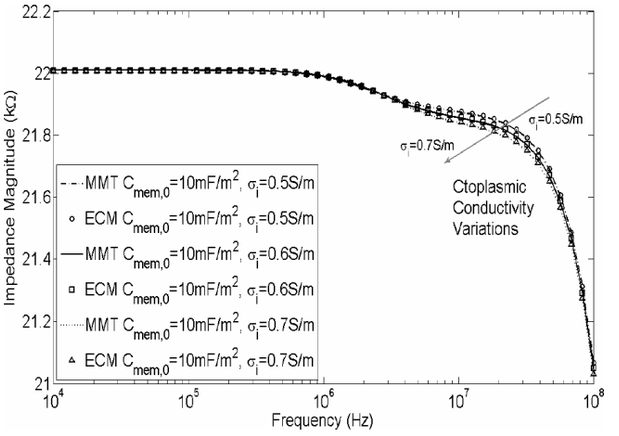

(b)

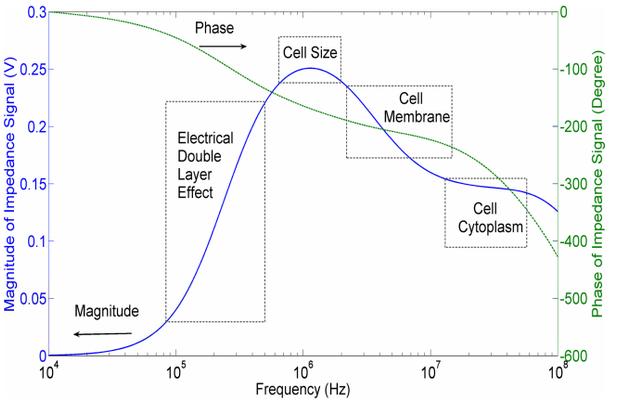

(c)

Fig. 4. Modeling of variations in the impedance magnitude spectra due to the changes in (a) cell specific membrane capacitance and (b) cell membrane capacitance using Maxwell's mixture theory (MMT) and equivalent circuit model (ECM). (c) Simulation of the impedance spectrum of single cell in differential mode using PSpice, magnitude (solid line) and phase (dashed line).

low frequency range (below 1 MHz), since the impedance of EDL is significantly high in that frequency range. The impedance spectra plotted in Figs. 4(a) and 4(b) do not consider the impedance of EDL in order to clearly show the β-relaxation in the radio-frequency. The influence of the impedance of EDL has been discussed in Ref. 30.

As stated before, one of the advantages of using ECM is that the simulations of the whole measurement system can be performed in commercial circuit analysis software by the combination with the differential measurement circuit schematic. Figure 4(c) shows the simulated impedance spectrum (magnitude and phase) in PSpice.

It should be pointed out that we use a differential mode measurement in the experiments to sense the impedance changes in the cytometer as a cell passes through the detection electrodes, as shown in Fig. 1. Therefore, the simulated impedance spectrum in Fig. 4(c) using PSpice differs from the impedance spectrum in Figs. 4(a) and 4(b). Because the impedance plotted in Fig. 4(c) is in the differential mode, which is expressed by:

$$\Delta\tilde{Z} = \tilde{Z}_{\text{mix\_DL}} - \tilde{Z}_{m\_\text{DL}}\,, \tag{15}$$

where $\Delta\tilde{Z}$ is the differential complex impedance. $\tilde{Z}_{\text{mix\_DL}}$ is the complex impedance of the suspending system including the EDL effect. $\tilde{Z}_{m\_\text{DL}}$ is the complex impedance of the pure medium between the two electrodes including the EDL effect.

In the circuit simulations, the value of the differential impedance, $\Delta\tilde{Z}$ is represented by the value of the output differential voltage signal. In Fig. 4(c), below 1 MHz, the effect of EDL results in the low sensitivity in differential impedance measurement, since most of the excitation voltage is dropped over the EDL. The maximum magnitude of the impedance depends on the size of the cell. Larger cells give higher impedance magnitude and are easier to be measured. As continuously increasing the frequency, the impedance spectrum gives the dielectric properties of the cell membrane and cytoplasm subsequently. According to our differential measurement circuit design, the cutoff (-3 dB) frequency is 50 MHz. This is limited by the characteristics of the operation amplifiers (such as: bandwidth, slew rate) in the circuit. Therefore, above 50 MHz, the magnitude of the impedance drops down due to the bandwidth of the circuit.

3.2. *Comparisons between MMT and FEM*

In this section, we compare the simulation results from MMT and FEM. In order to obtain the FEM simulations as accurate as possible, we have used a Dual AMD Opteron 250 64-bit computer with 8 GB RAM. The simulations were performed using Comsol Multiphysics 3.2 with a convergence set to 1×10^{-6}.

Firstly we consider the situation that the cell is located in the center of a cube ($20\,\mu\text{m} \times 20\,\mu\text{m} \times 20\,\mu\text{m}$), as shown in Fig. 5(a), with Neumann boundary condition $\partial\phi/\partial n = 0$ at the side walls (insulators) and Dirichlet boundary conditions on the top ($\phi = V$) and bottom ($\phi = 0$) surfaces (electrodes). The volume fraction is the ratio of the cell to cube volume. The cell is locating in a homogeneous electric field in this case, which guarantees the validity of using MMT.

The relative variation in the magnitude of the impedance, ΔZ_R, due to the presence of the cell is calculated as:

$$\Delta Z_R = \left|\frac{\Delta\tilde{Z}}{\tilde{Z}_m}\right|. \tag{16}$$

In Fig. 5(b), the value of ΔZ_R is plotted for low (1 kHz) and high (10 MHz) frequencies for both MMT and FEM (as a function of cell size). The impedance of the suspending system was calculated for different sized cells ($R = 1$ to $8\,\mu$m). It is evident that for the cube, the impedance calculated using MMT and FEM are in perfect agreement for all particle sizes simulated (up to 27% volume fraction). Generally, MMT is considered valid only at low volume fraction. For high concentrations of particles, the interaction between induced dipoles of particles should be taken into account, as described by Bruggeman[32] and Hanai.[28] The reason for better agreement in our simulations is likely due to the side boundary conditions in our case forcing the electric field close to the particle to be parallel, a different situation from large numbers of randomly distributed particles.

Then we come to the cytometer case. The cell is placed in the center, mid-way between the two electrodes as shown in Fig. 3(c). In this case, the electric field distribution is nonhomogeneous. This makes the application of MMT problematic, since the volume fraction cannot be calculated exactly. To a first approximation by ignoring the fringing field effect, the detection volume can be defined by the height

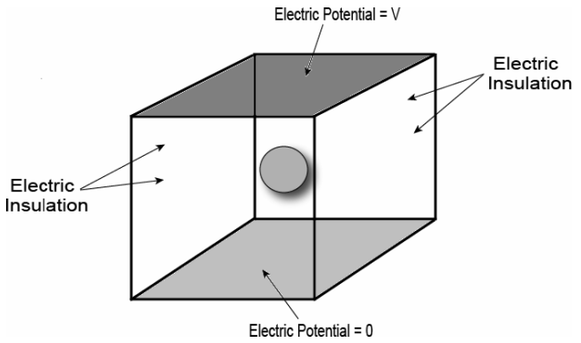

(a)

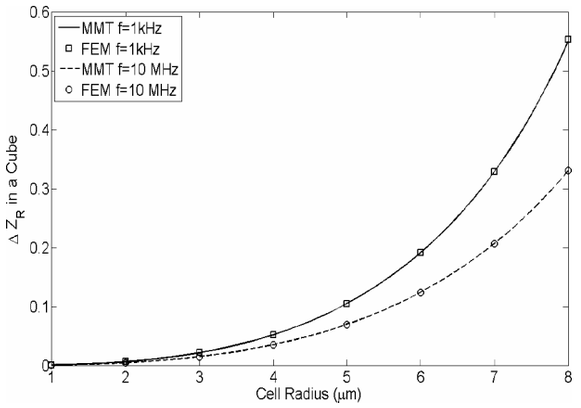

(b)

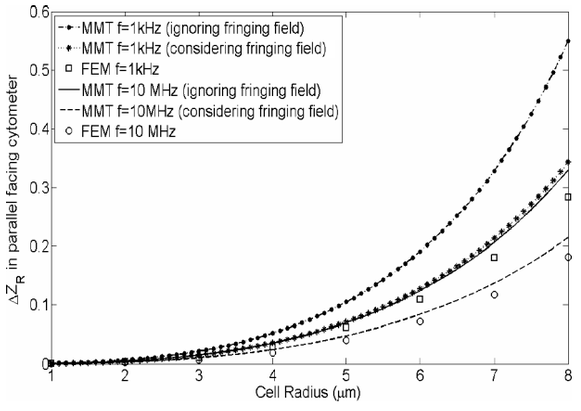

(c)

Fig. 5. (a) Diagram showing a single cell in suspension in a cube. The relative variation of the magnitude of the electrical impedance for a single cell in suspension (b) placed in a cube calculated by two methods; MMT and FEM and (c) located in the central of the cytometer, calculated by three methods: MMT (ignoring the fringing field effect), MMT (considering the fringing field effect), and FEM.

of the channel and the width and length of the electrode. In order to consider the fringing field effect, the cell constant of the device, κ, should be incorporated in the impedance calculations (Eqs. (4) and (5)). In Fig. 5(c), the difference in impedance, ΔZ_R, calculated using MMT for ignoring and considering the fringing field effect, and FEM is plotted for different cell sizes at low (1 kHz) and high (10 MHz) frequencies. This figure shows that using the cell constant to consider the fringing field effect in MMT gives a much better agreement with FEM than using the MMT by ignoring the fringing field effect. It can be observed that as the size of the cell increases, the discrepancy between the two methods also increases. This is because the fringing field effect becomes more serious, as the cell is larger.

These calculations and comparisons are made for a static cell located in the center of the system. Practically, the cell moves across the electrodes and, since the electric field varies along the channel, the current is also a function of the position of the cell in the channel. Therefore, the impedance of the system changes with the position of the cell. As a result, MMT is only suitable for calculating the maximum value in this dynamic process. The position dependent impedance of the system can only be evaluated by using FEM.

3.3. *Dynamic modeling — A moving cell*

The application of ECM and FEM can be combined together to model the variation of the differential impedance signal, as the cell is passing through the detecting electrodes. Figure 6 shows the 3D plot of the variation of the impedance signal dependent on the position of the cell and the frequency of the excitation voltage. The cell is moving along the central

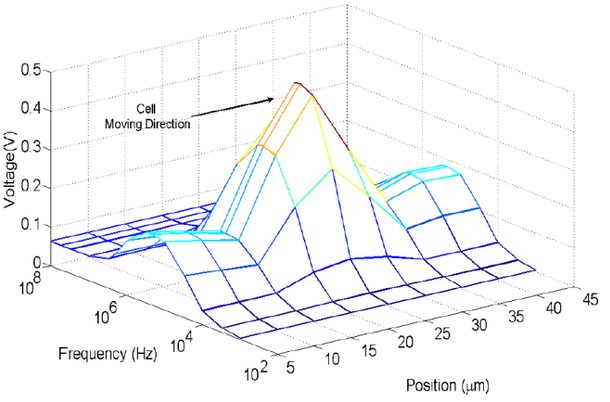

Fig. 6. 3D plot of the variation of the differential impedance signal as a function of the position of the cell and the frequency of the excitation voltage. The electrode is along the position-axis between 15 to 35 μm.

axis of the channel (midway between the two sides of the channel walls and also the top and bottom of the channel). Using the simulation parameters (for the cell and the chip) stated in the beginning of Sec. 3 and Eqs. (12)–(14), the impedance of the cell (resistance and capacitance) is firstly evaluated using FEM for different positions in the channel at different frequencies. Then the derived numerical solutions at discrete positions are imported into ECM (shown in Fig. 3(b)) to perform frequency-sweep circuit simulations in PSpice to obtain the respective impedance spectrum for the corresponding cell position.

4. Conclusion

We have presented three analytical or numerical methods to model the impedance of single cell in microfluidic cytometer, including Maxwell's mixture theory (MMT), equivalent circuit model (ECM) and finite element method (FEM). We have used these modeling methods to validate the experimental data and probed the dielectric properties of the measured biological cells.[30,33–35] In this paper, the impedance analysis is performed in the static case — the cell is locating in the center, between the two electrodes and also the dynamic case — the cell is moving along the channel. The validations of using these methods are verified by the comparisons between each other. The advantages and disadvantages of these three methods have been discussed, which are helpful for the researchers in this field to choose the optimal modeling tool for the specific work.

Acknowledgment

This work is partly supported by the Life Science Initiative, University of Southampton, UK.

References

1. H. Morgan and N. G. Green, *AC Electrokinetics: Colloids and Nanoparticles* (Research Studies Press, Ltd., Baldock, Hertfordshire, England, 2003).
2. H. Morgan, M. P. Hughes and N. G. Green, *J. Biophys.* **77**, 516 (1999).
3. N. G. Green, A. Ramos and H. Morgan, *J. Phys. D: Appl. Phys.* **33**, 632 (2000).
4. B. H. L. Encinas, B. A. Simmons, E. B. Cummings and Y. Fintschenko, *Anal. Chem.* **76**, 1571 (2004).
5. J. Voldman, *Ann. Rev. Biomed. Eng.* **8**, 425 (2006).
6. Y. Huang, X.-B. Wang, J. A. Tame and R. Pethig, *J. Phys. D: Appl. Phys.* **26**, 1528 (1993).
7. H. Morgan, N. G. Green, M. P. Hughes, W. Monaghan and T. C. Tan, *J. Micromech. Microeng.* **7**, 65 (1997).
8. L. Cui and H. Morgan, *J. Micromech. Microeng.* **10**, 72 (2000).
9. R. Hölzel, *J. Biophys.* **73**, 1103 (1997).
10. J. Yang, Y. Huang, X.-J. Wang, X.-B. Wang, F. F. Becker and P. R. C. Gascoyne, *J. Biophys.* **76**, 3307 (1999).
11. J. P. Huang, K. W. Yu, G. Q. Gu and M. Karttunen, *Phys. Rev. E* **67**, 1 (2003).
12. C. Dalton, A. D. Goater, J. P. H. Burt and H. V. Smith, *J. Appl. Microbio.* **96**, 24 (2004).
13. H. E. Ayliffe, A. B. Frazier and R. D. Rabbit, *IEEE Microelectromech. Syst.* **8**, 50 (1999).
14. L. L. Sohn, O. A. Saleh, G. R. Facer, A. J. Beavis, R. S. Allan and D. A. Notterman, *PNAS* **97**, 10687 (2000).
15. S. Gawad, L. Schild and Ph. Renaud, *Lab. Chip* **1**, 76 (2001).
16. S. Gawad, K. Cheung, U. Seger, A. Bertsch and Ph. Renaud, *Lab. Chip* **4**, 241 (2004).
17. B. F. D. Blasio, M. Laane, T. Walmann and I. Giaever, *Bio Techniques* **36**, 650 (2004).
18. K. Cheung, S. Gawad and Ph. Renaud, *Cytometry Part A* **65A**, 124 (2005).
19. H. Morgan, D. Holmes and N. G. Green, *Current Appl. Phys.* **6**, 367 (2006).
20. T. Sun, N. G. Green, S. Gawad and H. Morgan, *IET Nanobiotechnol.* **1**, 69 (2007).
21. D. Holmes, J. K. She, P. L. Roach and H. Morgan, *Lab. Chip* **7**, 1048 (2007).
22. H. Fricke, *J. Gen. Physiol.* **6**, 741 (1924).
23. H. Fricke, *Phys. Rev.* **24**, 575 (1924).
24. H. Fricke, *Phys. Rev.* **26**, 678 (1925).
25. J. C. Maxwell, *A Treatise on Electricity and Magnetism* (Dover, New York, 1954).
26. H. Pauly and H. P. Schwan, *Naturf. B* **14**, 125 (1959).
27. T. Sun, S. Gawad, N. G. Green and H. Morgan, *J. Phys. D: Appl. Phys.* **40**, 1 (2007).
28. T. Hanai, N. Koizumi and A. Irimajiri, *Biophys. Struct. Mech.* **1**, 285 (1975).
29. K. R. Foster and H. P. Schwan, *Rev. Biomed. Eng.* **17**, 25 (1989).
30. H. Morgan, T. Sun, D. Holmes, S. Gawad and N. G. Green, *J. Phys. D: Appl. Phys.* **40**, 61 (2007).
31. H. P. Schwan, *Adv. Biol. Med. Phys.* **5**, 147 (1957).
32. D. A. G. Bruggeman, *Ann. Phys. Lpz.* **24**, 636 (1935).
33. T. Sun, S. Gawad, C. Bernabini, N. G. Green and H. Morgan, *Meas. Sci. Tech.* **18**, 2859 (2007).
34. T. Sun, D. Holmes, S. Gawad, N. G. Green and H. Morgan, *Lab. Chip* **7**, 1034 (2007).
35. G. Benazzi, D. Holmes, T. Sun, M. Mowlem and H. Morgan, *IET Nanobiotechnol.* **1**, 94 (2007).

March 6, 2008 15:6 00080 fa1